

RESEARCH ARTICLE

Interplay between axonal Wnt5-Vang and dendritic Wnt5-Drl/Ryk signaling controls glomerular patterning in the *Drosophila* antennal lobeHuey Hing^{1*}, Noah Reger¹, Jennifer Snyder¹, Lee G. Fradkin²

1 Department of Biology, State University of New York at Brockport, Brockport, NY, United States of America, **2** Department of Neurobiology, University of Massachusetts Medical School, Worcester, MA, United States of America

* hhing@brockport.edu

OPEN ACCESS

Citation: Hing H, Reger N, Snyder J, Fradkin LG (2020) Interplay between axonal Wnt5-Vang and dendritic Wnt5-Drl/Ryk signaling controls glomerular patterning in the *Drosophila* antennal lobe. *PLoS Genet* 16(5): e1008767. <https://doi.org/10.1371/journal.pgen.1008767>

Editor: Ken M. Cadigan, University of Michigan, UNITED STATES

Received: November 29, 2019

Accepted: April 8, 2020

Published: May 1, 2020

Copyright: © 2020 Hing et al. This is an open access article distributed under the terms of the [Creative Commons Attribution License](https://creativecommons.org/licenses/by/4.0/), which permits unrestricted use, distribution, and reproduction in any medium, provided the original author and source are credited.

Data Availability Statement: All relevant data are within the manuscript and its Supporting Information files.

Funding: This work was supported by grants from the NIH/NIDCD (DC010916-02A1) awarded to HH. The funders had no role in study design, data collection and analysis, decision to publish, or preparation of the manuscript.

Competing interests: The authors have declared that no competing interests exist.

Abstract

Despite the importance of dendritic targeting in neural circuit assembly, the mechanisms by which it is controlled still remain incompletely understood. We previously showed that in the developing *Drosophila* antennal lobe, the Wnt5 protein forms a gradient that directs the ~45° rotation of a cluster of projection neuron (PN) dendrites, including the adjacent DA1 and VA1d dendrites. We report here that the Van Gogh (Vang) transmembrane planar cell polarity (PCP) protein is required for the rotation of the DA1/VA1d dendritic pair. Cell type-specific rescue and mosaic analyses showed that Vang functions in the olfactory receptor neurons (ORNs), suggesting a codependence of ORN axonal and PN dendritic targeting. Loss of Vang suppressed the repulsion of the VA1d dendrites by Wnt5, indicating that Wnt5 signals through Vang to direct the rotation of the DA1 and VA1d glomeruli. We observed that the Derailed (Drl)/Ryk atypical receptor tyrosine kinase is also required for the rotation of the DA1/VA1d dendritic pair. Antibody staining showed that Drl/Ryk is much more highly expressed by the DA1 dendrites than the adjacent VA1d dendrites. Mosaic and epistatic analyses showed that Drl/Ryk specifically functions in the DA1 dendrites in which it antagonizes the Wnt5-Vang repulsion and mediates the migration of the DA1 glomerulus towards Wnt5. Thus, the nascent DA1 and VA1d glomeruli appear to exhibit Drl/Ryk-dependent biphasic responses to Wnt5. Our work shows that the final patterning of the fly olfactory map is the result of an interplay between ORN axons and PN dendrites, wherein converging pre- and postsynaptic processes contribute key Wnt5 signaling components, allowing Wnt5 to orient the rotation of nascent synapses through a PCP mechanism.

Author summary

During brain development, the processes of nerve cells, axons and dendrites, grow over long distances to find and connect with each other to form synapses in precise locations. Understanding the mechanisms that control the growth of these neurites is important for

understanding normal brain functions like neuronal plasticity and neural diseases like autism. Although much progress has been made by studying the development of axons and dendrites separately, the mechanisms that guide neuronal processes to their final locations are still incompletely understood. In particular, careful observation of converging pre- and postsynaptic processes suggests that their targeting may be coordinated. Whether the final targeting of axons and dendrites are functionally linked and what molecular mechanisms may be involved are unknown. In this paper we show that, in the developing *Drosophila* olfactory circuit, coalescing axons and dendrites respond to the extracellular Wnt5 signal in a codependent manner. We demonstrate that the converging axons and dendrites contribute different signaling components to the Wnt5 pathway, the Vang Gogh and Derailed transmembrane receptors respectively, which allow Wnt5 to coordinately guide the targeting of the neurites. Our work thus reveals a novel mechanism of neural circuit patterning and the molecular mechanism that controls it.

Introduction

The prevailing view of neural circuit assembly is that axons and dendrites are separately guided by molecular gradients to their respective positions whereupon they form synapses with each other [1–4]. However, careful observation of developing neural circuits reveals that the process may be more complex. For example, in the developing retina outer plexiform layer (OPL) the axon terminals of rods and cones, and dendrites of their respective postsynaptic cells, the rod and cone bipolar cells, are initially intermingled in the nascent OPL [5]. Even as the rod and cone axons are connecting with their target dendrites, the terminals are segregating into rod- and cone-specific sub-laminae, suggesting that the processes of targeting and synaptic partner matching may be coordinated. Whether the two processes are functionally linked and what mechanisms might be involved are unknown.

The stereotyped neural circuit of the *Drosophila* olfactory map offers a unique opportunity to unravel the mechanisms of neural circuit development. Dendrites of 50 classes of uniglomerular projection neurons (PNs) form synapses with the axons of 50 classes of olfactory receptor neurons (ORNs) in the antennal lobe (AL) in unique glomeruli [6, 7]. This precise glomerular map is thought to be established during the pupal stage by the targeting of PN dendrites [8–10]. We previously reported that during the establishment of the fly olfactory map, two adjacent dendritic arbors located at the dorsolateral region of the AL, the DA1 and VA1d dendrites (hereafter referred to as the DA1/VA1d dendritic pair), undergo rotational migration of $\sim 45^\circ$ around each other to attain their final adult positions [11]. This rearrangement (in the lateral/ $90^\circ \rightarrow$ dorsal/ $0^\circ \rightarrow$ medial/ $270^\circ \rightarrow$ ventral/ 180° direction) occurs between 16 and 30 hour After Puparium Formation (hAPF), a period of major ORN axon ingrowth to the AL [8, 12, 13]. We showed that a Wnt5 signal guides this rotation by repelling the dendrites [11]. Wnt5 is expressed by a set of AL-extrinsic cells and forms a dorsolateral-high to ventromedial-low (DL > VM) gradient in the AL neuropil which provides a directional cue to align the dendritic pattern relative to the axes of the brain. We also showed that the Derailed (Drl)/Ryk kinase-dead receptor tyrosine kinase, a Wnt5 receptor [14–17], is differentially expressed by the PN dendrites, thus providing cell-intrinsic information for their targeting in the Wnt5 gradient. Interestingly, *drl* opposes *Wnt5* repulsive signaling so that dendrites expressing high levels of *drl* terminate in regions of high *Wnt5* concentration and *vice versa*. To further unravel the mechanisms of PN dendritic targeting, we have screened for more mutations that disrupt the rotation of the DA1/VA1d dendritic pair.

Here we report that mutations in the *Van Gogh* (*Vang*) gene disrupted the rotation of the DA1/VA1d dendritic pair, thus mimicking the *Wnt5* mutant phenotype. *Vang* encodes a four-pass transmembrane protein [18, 19] of the core Planar Cell Polarity (PCP) group, an evolutionarily conserved signaling module that imparts polarity to cells [20, 21]. The loss of *Vang* suppressed the repulsion of the VA1d dendrites by *Wnt5*, indicating that *Vang* is a downstream component of *Wnt5* signaling. Surprisingly, *Vang* acts in the ORNs, which suggests an obligatory codependence of ORN axon and PN dendritic migration. We also show that the *drl* gene is selectively expressed in the DA1 dendrites where it antagonizes *Vang* and appears to convert *Wnt5* repulsion of the DA1 glomerulus into attraction. The opposing responses of the DA1 and VA1d glomeruli likely create the forces by which *Wnt5* directs the rotation of the glomerular pair. Our work shows that converging pre- and postsynaptic processes contribute key signaling components of the *Wnt5* pathway, allowing the processes to be co-guided by the *Wnt5* signal.

Results

Vang promotes the rotation of DA1/VA1d dendrites

We have shown that during wild-type development the adjacent DA1 and VA1d dendrites rotate around each other, such that DA1 moves from its original position lateral to VA1d at 18 hAPF to its final position dorsolateral to VA1d in the adult, an $\sim 45^\circ$ rotation [11]. We also showed that this rotation requires the *Wnt5* gene, for in the null *Wnt5*⁴⁰⁰ mutant the rotation is abolished, resulting in an adult DA1/VA1d angle of $76.03^\circ \pm 3.6^\circ$ (N = 29, vs $29.32^\circ \pm 2.5^\circ$, N = 22 in the *Wnt5*^{400/+} heterozygous control, Student's *t* test $p < 0.0001$) (See [Materials and Methods](#) and [S1 Fig](#) for quantification) ([Fig 1A–1C](#)). The DA1 and VA1d pair of dendrites were visualized by expressing *UAS-mCD8::GFP* under the control of *Mz19-Gal4*, which specifically labels the DA1, VA1d and DC3 dendrites [22, 23]. To elucidate the molecular mechanisms by which *Wnt5* controls the rotation of the PN dendrites, we screened a panel of signal transduction mutants for similar defects in DA1/VA1d rotation. We found that animal homozygous for *Vang* mutations exhibit a DA1/VA1d phenotype that mimicked that of the *Wnt5*⁴⁰⁰ mutant. For example, in the null *Vang*⁶ allele, the DA1/VA1d angle was $54.72^\circ \pm 2.8^\circ$ (N = 24, vs $27.78^\circ \pm 4.6^\circ$, N = 18 in the *Vang*^{6/+} heterozygous control, *t*-test $p < 0.0001$) ([Fig 1D–1F](#)) suggesting that *Vang* might function in the *Wnt5* pathway. Since the *Vang*⁶ allele, which encodes a truncated 128 amino acid product [19], displayed a highly penetrant phenotype, we examined this allele further. We therefore examined the positioning of glomeruli in different regions of the *Vang*⁶ AL by expressing *UAS-mCD8::GFP* under the control of various *Or-Gal4* drivers [6] ([Fig 1G–1O](#), see [Materials and Methods](#) for quantification). We observed that glomeruli in the lateral region of the AL, such as the VA1v glomerulus ([Fig 1G–1I](#)), showed the greatest displacement compared with glomeruli in other regions, suggesting that *Vang* primarily controls neurite targeting in the lateral AL. Since the *Wnt5* protein is highly concentrated at the dorsolateral region of the AL [11], the *Vang* mutant defects are consistent with *Vang* playing a role in *Wnt5* signaling. We hypothesized that *Vang* mediates *Wnt5* signaling in the control of the DA1/VA1d dendritic rotation.

To obtain further evidence for *Vang*'s role in regulating the rotation of the DA1/VA1d dendritic pair, we stained ALs during a time of active glomerular rotation (24 hAPF) [11] with an antibody directed against the N-terminal 143 amino acids of *Vang* [24]. We observed that the *Vang* staining has a punctate appearance and is highly concentrated in the dorsolateral region of the AL between 0–9 μm from the AL anterior surface ([Fig 2A](#)). Co-labeling of the DA1/VA1d dendrites with the *Mz19-Gal4* driver showed that they reside between ~ 3 –6 μm in this high *Vang* expression domain. *Vang* staining in the neuropil begins to decline at 10 μm but

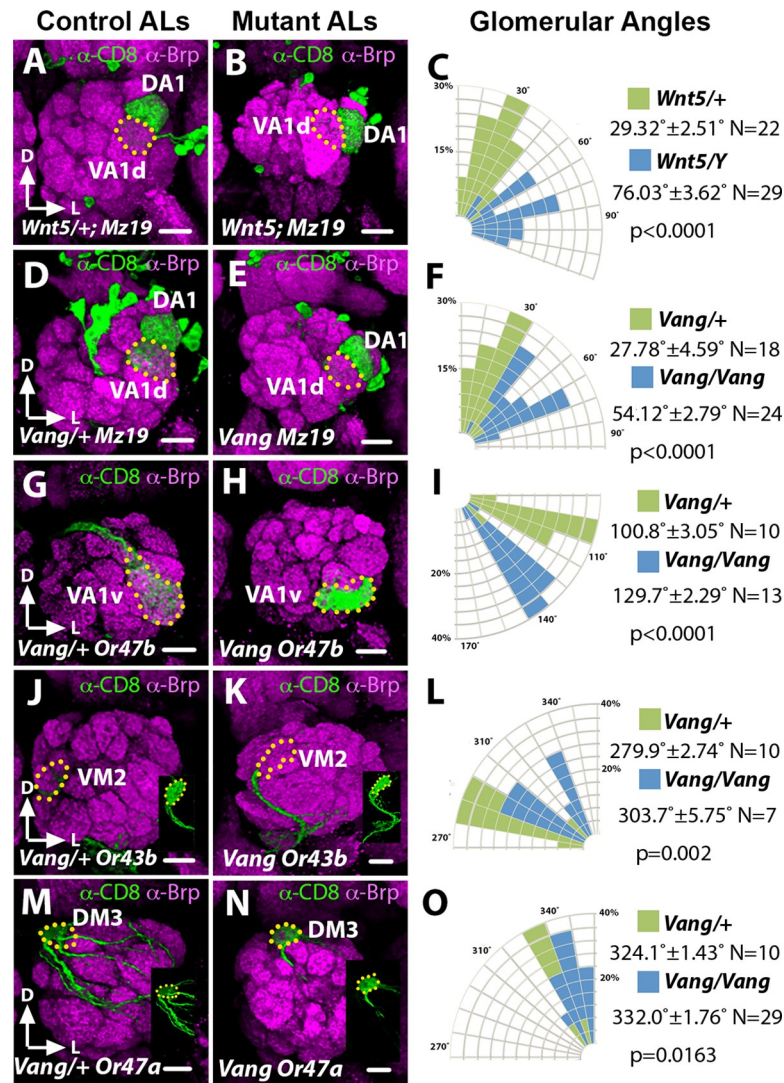


Fig 1. The *Vang*⁶ mutant AL defects mimic that of the *Wnt5*⁴⁰⁰ mutant. Frontal views of the left ALs are shown (dorsal up and lateral to the right) in this and following figures. (A-F) Adult ALs from animals expressing *UAS-mCD8::GFP* under the control of *Mz19-Gal4* stained with antibodies against Bruchpilot (Brp, Magenta) to highlight the AL neuropil and CD8 (green) to highlight the DA1 and VA1d PN dendritic arbors in the *Wnt5*⁴⁰⁰/*+* (A) and *Vang*⁶/*+* (D) controls, and *Wnt5*⁴⁰⁰ (B) and *Vang*⁶ (E) mutants. (C, F) Quantification of the DA1/VA1d angles in the *Wnt5*⁴⁰⁰ and *Vang*⁶ mutants respectively. The DA1 dendrites are located dorsal to the VA1d dendrites in the controls but lateral to the VA1d dendrites in the *Wnt5*⁴⁰⁰ and *Vang*⁶ mutants. (G-O) Left adult ALs from animals expressing *UAS-mCD8::GFP* under the control of *Or47b-Gal4* (G, H), *Or43b-Gal4* (J, K) and *Or47a-Gal4* (M, N) to label lateral, medial and dorsal glomeruli respectively, in the *Vang*⁶/*+* (G, J, M) controls and *Vang*⁶ mutants (H, K, N). (I, L, O) Quantification of the positions of the *Or47b*, *Or43b* and *Or47a* glomeruli respectively in the control vs *Vang*⁶ animals. The glomeruli appeared to be displaced in the clockwise direction in the *Vang*⁶ mutant, with VA1v showing the greatest displacement. Insets (J, K, M, N) show the ORN terminals in the absence of Brp staining. Student's *t* tests were used to compare the data of the mutants with those of their respective controls. Scale bars: 10 μ m.

<https://doi.org/10.1371/journal.pgen.1008767.g001>

strongly highlighted the nerve fiber layer (arrow) and the antennal nerve at 8–12 μ m (arrow and arrowheads in Fig 2A and 2B), as well as the antennal commissure at 22 μ m depth. The antibody stained the *Vang*⁶ mutant ALs (Fig 2C), likely because the *Vang*⁶ allele encodes a truncated protein. Nonetheless, the strong reduction in staining intensity compared with wild-type ALs attested to the antibody's specificity. We concluded that Vang is expressed in the AL during the period of active AL neuropil rotation, where it colocalized with the DA1 and VA1d

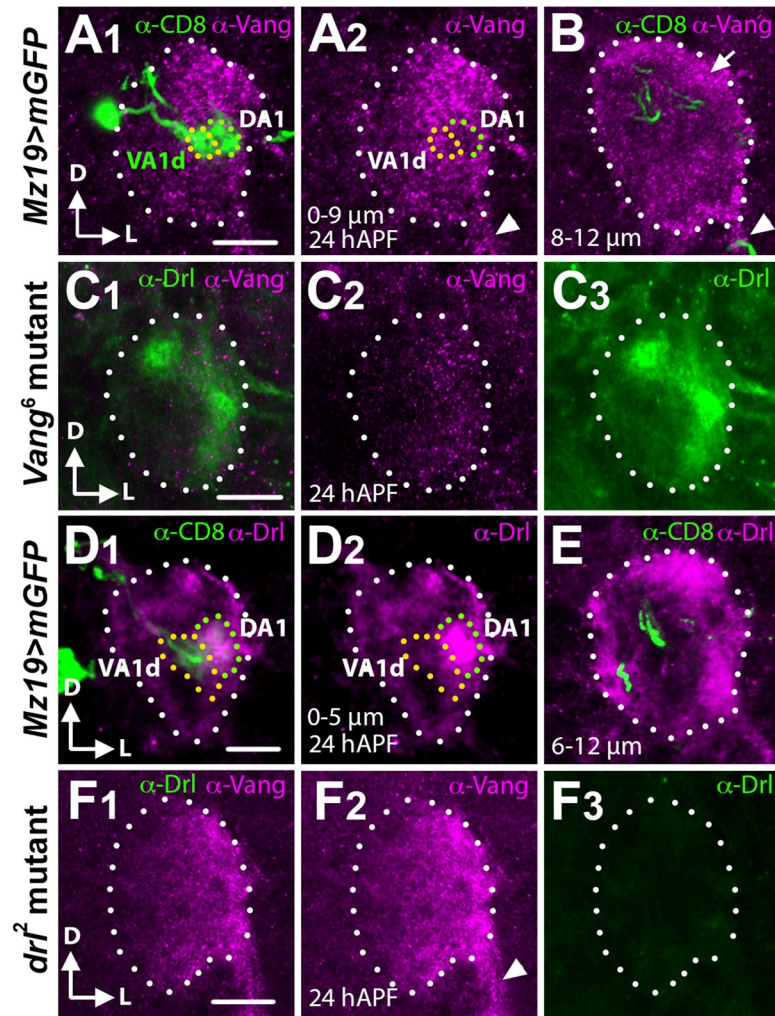


Fig 2. The Vang and Drl expression domains overlap with the developing DA1 and VA1d dendrites. Frontal views of 24 hAPF ALs stained with Vang and Drl antibodies. (A, B) An AL from animals expressing *UAS-mCD8::GFP* under the control of *Mz19-Gal4* stained with antibodies against Vang (Magenta) and CD8 (green) to highlight the DA1 and VA1d PN dendritic arbors. Between 0–9 μm from the anterior AL surface Vang is found in puncta, which are highly concentrated in the AL dorsolateral region where the DA1 and VA1d dendrites are localized (A₁, A₂). In deeper sections (8–12 μm) Vang is observed in the nerve fiber layer (arrow) and the antennal nerve (arrowhead) (B). (C) An AL from *Vang*⁶ mutants stained with antibodies against Vang (Magenta) and Drl (green) (C₁). The AL stained poorly for Vang (C₂) but strongly for Drl (C₃) attesting to the specificity of the Vang antibody. (D, E) An AL from animals expressing *UAS-mCD8::GFP* under the control of *Mz19-Gal4* stained with antibodies against Drl (Magenta) and CD8 (green). From 0–5 μm the Drl protein is concentrated in the lateral AL where it co-localizes with the DA1 dendrites (D₁, D₂). The VA1d dendrites are located medially and express a low level of the Drl protein. Deeper down (5–12 μm) the Drl protein is found in the dorsal and ventrolateral neuropil structures (E). (F) An AL from *drl*² mutants stained with antibodies against Vang (Magenta) and Drl (green) (F₁). The AL stained strongly for Vang (F₂) but not at all for Drl (F₃) attesting to the specificity of the Drl antibody. Scale bars: 10 μm .

<https://doi.org/10.1371/journal.pgen.1008767.g002>

dendrites. The Vang expression pattern is consistent with the hypothesis that *Vang* mediates *Wnt5* control of the DA1/VA1d dendritic rotation.

Vang is required in the ORNs for DA1-VA1d dendritic rotation

Since the Vang antibody strongly stained the AL nerve fiber layer, the antennal nerve and the antennal commissure, we hypothesized that Vang is expressed by ORNs and carried by axons

to the developing AL. To identify the cell type in which *Vang* functions, we first used transgenic techniques to modulate *Vang* activity in specific cell types and examined the effect on the DA1/VA1d dendritic rotation. When we expressed the *UAS-Vang* transgene with the *Elav-Gal4* pan-neuronal driver [25] in the *Vang^Δ* mutant, the DA1/VA1d dendritic angles became smaller ($32.88^\circ \pm 2.19^\circ$, $N = 24$) compared with that of the mutant control ($51.40^\circ \pm 3.39^\circ$, $N = 20$, t -test $p < 0.0001$), indicating that *Vang* functions in neurons to promote dendritic rotation (Fig 3A–3C and 3M). When we expressed *UAS-Vang* using the ORN-specific drivers, *peb-Gal4* and *SG18.1-Gal4*, the DA1/VA1d dendritic angles were also reduced ($29.18^\circ \pm 1.6^\circ$, $N = 37$ and $32.12^\circ \pm 2.12^\circ$, $N = 58$ respectively) compared with that of the *Vang^Δ* mutant ($60.82^\circ \pm 2.52^\circ$, $N = 17$, *peb* rescue vs. *Vang^Δ*, $p < 0.0001$; *SG18.1* rescue vs. *Vang^Δ*, $p < 0.0001$; *peb* rescue vs. *SG18.1* rescue, $p = 0.8283$; one-way ANOVA with post hoc Tukey test), indicating that *Vang* acts in the ORNs (Fig 3D–3I and 3M). In contrast, expression of *UAS-Vang* using a PN-specific driver, *GH146-Gal4*, did not significantly alter the DA1/VA1d rotational angles of the *Vang^Δ* mutant ($47.87^\circ \pm 2.21^\circ$, $N = 39$, t -test $p = 0.3894$; Fig 3M). In further support of *Vang* acting in the ORNs, when we drove the *UAS-Vang^{RNAi}* transgene [26] in the *Vang^Δ/+* heterozygote with *peb-Gal4*, the rotation of the DA1/VA1d dendritic angle increased slightly compared with that of the *Vang^Δ/+* heterozygote, indicating that *Vang* is required in the ORNs for DA1/VA1d dendritic rotation ($36.40^\circ \pm 2.93^\circ$, $N = 24$ compared with $30.09^\circ \pm 1.01^\circ$, $N = 22$, t -test $p = 0.0518$) (Fig 3J–3L and 3N).

To confirm the above findings, we used mosaic techniques to induce ORNs or PNs lacking the *Vang* gene and examined the effects on the DA1/VA1d dendritic rotation. Induction of either *Vang^{f04290}* or *Vang^Δ* mutant ORN axons using the *ey-FLP/FRT* technique, which induces large clones in the antenna [27], resulted in the DA1/VA1d dendritic pair exhibiting larger angles ($54.73^\circ \pm 3.26^\circ$, $N = 30$ and $51.03^\circ \pm 2.62^\circ$, $N = 28$ respectively) compared with animals innervated by wild-type ORN axons ($20.24^\circ \pm 2.51^\circ$, $N = 20$, wild type vs. *Vang^{f04290}*, $p < 0.0001$; wild type vs. *Vang^Δ*, $p < 0.0001$; *Vang^Δ* vs. *Vang^{f04290}*, $p = 0.7297$; one-way ANOVA with post hoc Tukey test) (Fig 4A–4C, 4G and 4H), confirming that *Vang* is required in the ORNs for DA1/VA1d dendritic rotation. Next, we induced *Vang^Δ* mutant PN clones using the MARCM system [28] with *GH146-Gal4* as the PN marker. We observed that *Vang^Δ* mutant PN neuroblast and single-cell clones extended their dendrites into AL and innervated the glomeruli normally (Fig 4D–4F). Importantly, ALs innervated by large *vang^Δ* PN clones exhibited normal dendritic pattern, as judged by the angles of the DA1/VA1d dendrites ($27.50^\circ \pm 4.89^\circ$, $N = 12$) compared with those of the control ($23.29^\circ \pm 5.27^\circ$, $N = 7$, t -test $p = 0.56$) (Fig 4E, 4G and 4H). Thus, our transgenic rescue and mosaic experiments showed that *Vang* functions in the ORNs to non-autonomously promote the rotation of the DA1/VA1d dendritic pair.

Vang is not required for ORN axon growth or correct ORN-PN pairing

A possible explanation for the *Vang* mutant phenotype is that *Vang* is required for ORN axon growth to the AL, the failure of which indirectly disrupted glomerular patterning. Mutations in *Vang* have been shown to result in abnormal projection of mushroom body axons [29]. To determine if ORN axons entered the AL in the *Vang^Δ* mutant, we labeled eight different ORN axon terminals in the AL using *Or-Gal4* drivers. We found that *Vang^Δ* mutant axons entered the AL normally, although their terminals were shifted in the AL neuropil (Fig 1). To investigate if the *Vang* mutation disrupted the proper matching of the ORN axons and PN dendrites, we simultaneously labeled pre- and postsynaptic partners of glomeruli for which specific markers were available. We achieved this by labeling the DA1, VA1d and DM1 dendrites with *Mz19-Gal4* driving *UAS-mCD8::GFP* and simultaneously the ORN axons targeting the VA1d and VA1v glomeruli with the *Or88a-CD2* and *Or47b-CD2* transgenes respectively. We

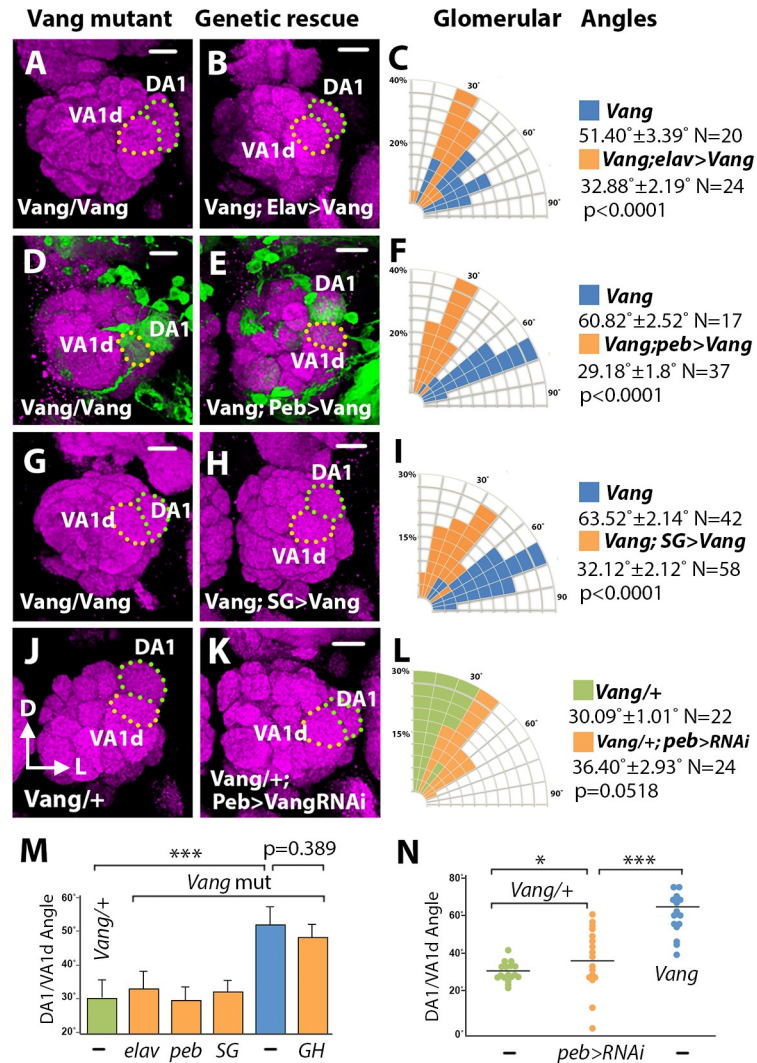


Fig 3. *Vang* functions in the ORNs to regulate glomerular migration. Adult *Vang*⁶ ALs expressing *Mz19-mCD8::GFP* and different *Vang* transgenes were stained with antibodies against Brp (Magenta) and CD8 (green) to visualize the glomerular pattern. (A, B) Expression of *UAS-Vang* under the control of the pan-neuronal driver *Elav-Gal4* in the *Vang*⁶ mutant (A) caused DA1 to migrate dorsally relative to the VA1d glomerulus (B). (C) Quantification of the DA1/VA1d glomerular angles in A and B. (D, E, G, H) Expression of *UAS-Vang* under the control of the ORN-specific drivers, *peb-Gal4* (D, E) and *SG18.1-Gal4* (G, H), also rescued DA1 dorsal migration. (F, I) Quantification of the DA1/VA1d glomerular angles in D, E, G, and H. (J, K) Expression of *UAS-Vang^{RNAi}* under the control of the *peb-Gal4* in the *Vang*^{6/+} mutant (J) slightly disrupted DA1 dorsal migration (K). (L) Quantification of the DA1/VA1d glomerular angles in the rescue experiments. (M) Graph summarizing the glomerular angles in the rescue experiments. ANOVAs were used to simultaneously compare the *Vang*⁶ control and the rescued conditions. (N) Graph summarizing the glomerular angles in the *Vang*^{RNAi} knockdown experiment. With the exception of M, Student's *t* tests were used to compare the data of the mutants with those of their respective controls. Scale bars: 10 μm.

<https://doi.org/10.1371/journal.pgen.1008767.g003>

observed that *Or88a* axons were strictly paired with VA1d PN dendrites in the *Vang*⁶ mutant as in the wild type (Fig 5A and 5B). Likewise, the *Or47b* axons strictly innervated the VA1v glomerulus, and never strayed into the VA1d territory in the *Vang*⁶ mutant (Fig 5C). Thus, *Vang* is not required for ORN axon projection into the AL or their correct pairing with their postsynaptic partners. We propose that *Vang* functions in the context of paired axons and dendrites allowing the neurites to coordinately respond to the *Wnt5* signal. This idea is consistent

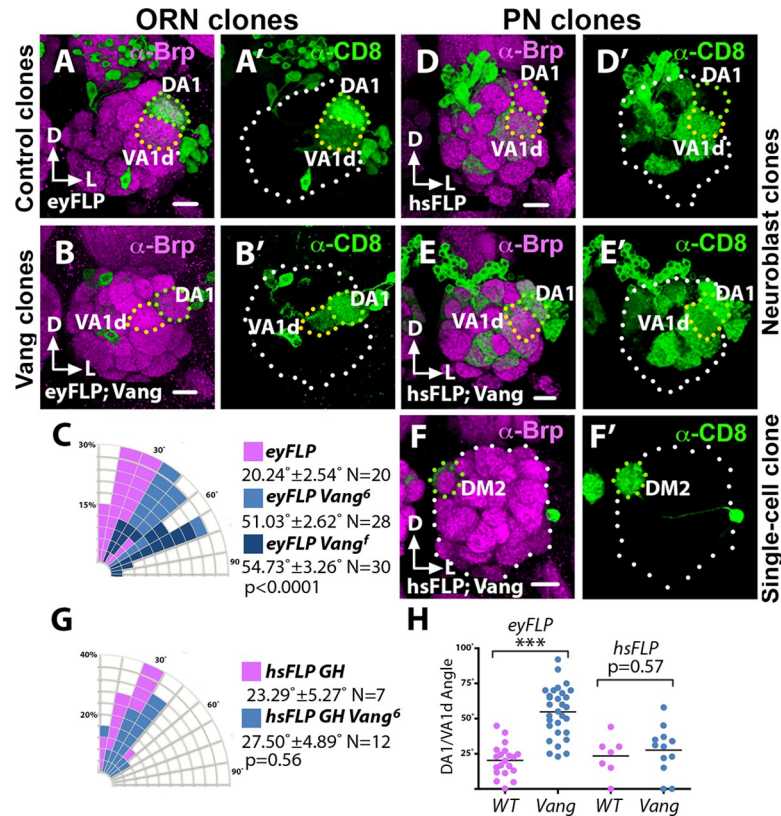


Fig 4. *Vang* functions selectively in ORNs but not the PNs to regulate glomerular migration. *Vang*⁶ and control mosaic ALs were stained with antibodies against Brp (Magenta) to visualize the glomerular pattern and CD8 (green) to visualize PN dendritic arborization. (A) In ALs innervated by wild-type ORN axon clones induced by the *ey-FLP/FRT* technique the DA1 glomerulus migrated normally relative to the VA1d glomerulus. (B) In ALs innervated by *Vang*⁶ mutant axon clones induced by the *ey-FLP/FRT* technique the DA1 glomerulus failed to migrate dorsally relative to the VA1d glomerulus. (C) Quantification of the glomerular angles in A and B. ANOVAs were used to simultaneously compare the control and the *Vang*⁶ and *Vang*⁰⁴²⁹⁰ conditions. (D) In ALs innervated by large clones of wild-type PN dendrites, induced by the MARCM technique the DA1 glomerulus migrated normally relative to the VA1d glomerulus. (E, F) In ALs innervated by neuroblast (E) and single-cell (F) clones of *Vang*⁶ PN dendrites induced by the MARCM technique, the mutant dendrites innervated the AL normally and the DA1 glomerulus migrated normally relative to the VA1d glomerulus. (G) Quantification of the glomerular angles in D, E and F. Student's *t* test was used to compare the data of the mutant clones with that of the controls. (H) Graph summarizing the glomerular angles in the mosaic control and *Vang*⁶ ALs. Scale bars: 10 μ m.

<https://doi.org/10.1371/journal.pgen.1008767.g004>

with our observation that PN dendritic rotation occurs between 16 and 30 hAPF [11], the period of major ORN axon invasion into the AL [8, 12].

Vang acts downstream of *Wnt5* to repel the VA1d glomerulus

The close resemblance of the *Vang* and *Wnt5* mutant phenotypes raised the questions of whether and how *Vang* might function in the *Wnt5* signaling pathway to regulate the rotation of the DA1 and VA1d glomeruli. To address these questions, we asked if loss of *Vang* would block *Wnt5* signaling. We previously showed that overexpression of *Wnt5* in the DA1 and VA1d dendrites with the *Mz19-Gal4* driver split the VA1d dendrites into two smaller arbors probably due to repulsion between the dendrites (Fig 6A and 6B) [11]. Interestingly, *Wnt5* overexpression had no effect on the DA1 dendrites, indicating that the DA1 and VA1d dendrites respond differentially to the *Wnt5* signal. The VA1d defect provided an opportunity to

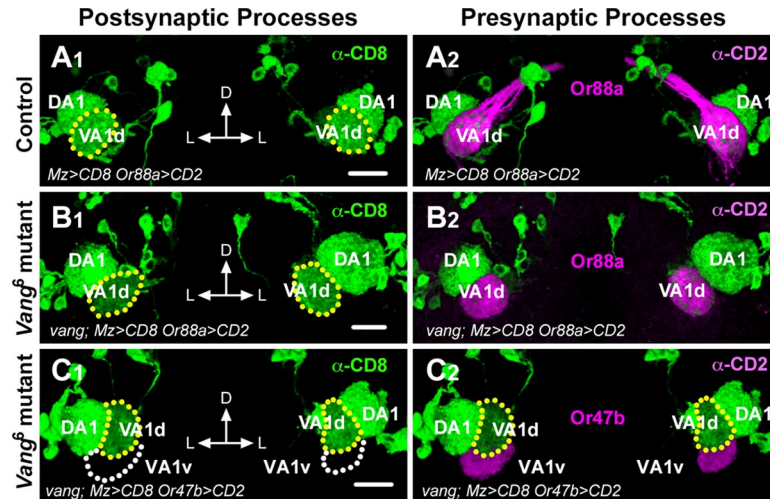


Fig 5. *Vang* does not function in ORN axon projection or pairing with cognate PN dendritic partners. (A, B) Adult brains from animals expressing *Or88a-CD2* and *UAS-mCD8::GFP* under the control of *Mz19-Gal4* were stained with anti-CD2 (magenta) and anti-CD8 (green) to visualize the pre- and postsynaptic processes of the VA1d and VA1v glomeruli. In the wild-type control, *Or88a* axons are faithfully paired with the VA1d dendrites (A). Collaterals form a fascicle, which innervates the contralateral AL. In the *Vang*⁶ mutant, *Or88a* axons are also faithfully paired with the VA1d dendrites (B). *Vang* mutant axons fail to sprout collaterals as previously reported [29]. (C) Frontal views of adult ALs from *Vang*⁶ mutants expressing *Or47b-CD2* and *UAS-mCD8::GFP* under the control of *Mz19-Gal4* stained with anti-CD2 (magenta) and anti-CD8 (green). In the mutant, *Or47b* axons targeted the adjacent VA1v glomerulus without straying into the VA1d glomerular territory. Scale bar: 10 μ m.

<https://doi.org/10.1371/journal.pgen.1008767.g005>

assess if *Vang* is needed for the *Wnt5* gain-of-function phenotype. Whereas only 9.37% (3/32) of the VA1d dendrites in the *Mz19>Wnt5* animals were intact, this fraction rose to 45.65% (21/46) in the *Mz19>Wnt5; Vang*⁶/*Vang*⁶ animals (Fig 6C and 6F). Moreover, the distances between the split VA1d arbors in the *Mz19>Wnt5; Vang*⁶/*Vang*⁶ animals were smaller than those in the *Mz19>Wnt5* animals (11.83 μ m \pm 0.61 μ m, N = 25, vs 21.06 μ m \pm 0.96 μ m, N = 29, *t*-test *p* < 0.0001) (Fig 6B, 6C and 6G). Despite severe distortion, the VA1d dendrites were faithfully paired with their *Or88a* axon partners, reinforcing the idea that *Wnt5* signaling does not play a role in ORN-PN matching (Fig 6D and 6E). Overexpression of *Wnt5* in the DA1 and VA1d dendrites did not affect the development of the *Or88a* neurons (S2 Fig). We conclude that *Wnt5* signals through *Vang* to repel the VA1d glomerulus.

To further probe the relationship between *Wnt5* and *Vang*, we examined the DA1/VA1d rotation in animals lacking both genes. We observed that the rotation in the *Wnt5*⁴⁰⁰; *Vang*⁶ double mutant (92.20° \pm 4.1°, N = 41) is more severely disrupted than that in either single mutant (76.03° \pm 3.62° in *Wnt5*⁴⁰⁰, n = 29, *t*-test *p* = 0.0031 and 54.12° \pm 2.8° in *Vang*⁶, n = 34, *t*-test *p* < 0.0001) (Fig 7). The enhanced phenotype of the *Wnt5*⁴⁰⁰; *Vang*⁶ mutant suggested that *Wnt5* and *Vang* could function independently to promote DA1/VA1d rotation (Fig 7F). We currently do not know how *Vang* acts independently of *Wnt5*. However, it is interesting that *Wnt5* directs the rotation of the DA1/VA1d glomeruli through both *Vang*-dependent and *Vang*-independent pathways. Since *Wnt5* acts through *Vang* in the VA1d glomerulus, we hypothesized that *Wnt5* acts through a *Vang*-independent mechanism in the DA1 glomerulus.

***drl* promotes the rotation of DA1-VA1d glomeruli**

The Drl atypical receptor tyrosine kinase has been shown to bind *Wnt5* and mediates its signaling in the migration of a number of cell types [14–17]. We previously demonstrated that

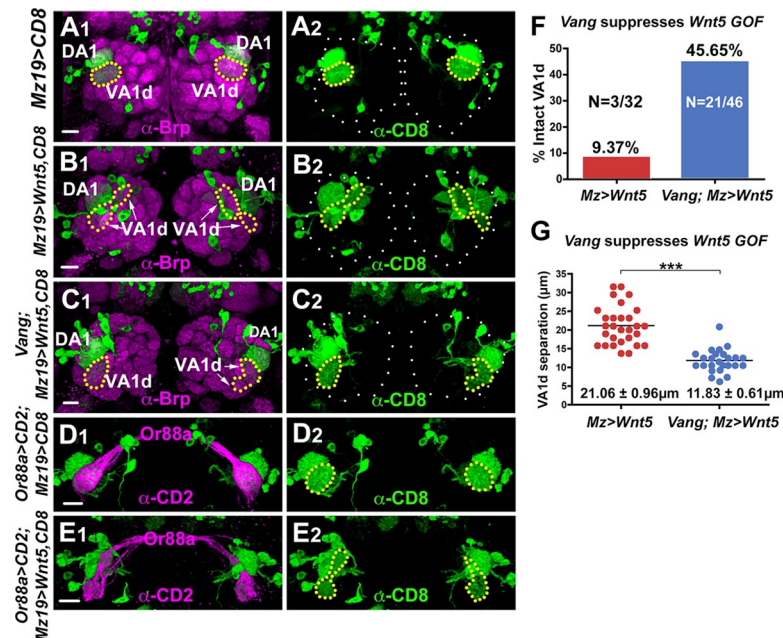


Fig 6. Vang functions downstream of Wnt5 to cell non-autonomously repel the VA1d dendrites. (A–C) Adult ALs from animals expressing *UAS-mCD8::GFP* under the control of *Mz19-Gal4* were stained with antibodies against Brp (magenta) to visualize the glomerular pattern and CD8 to visualize the DA1/VA1d dendrites (green). (A) In the wild-type control, the DA1 dendrites are located dorsal to the VA1d dendrites, which form a single compact arbor. (B) In animals expressing *UAS-Wnt5* under the control of *Mz19-Gal4*, the VA1d dendrites split into two separated arbors, probably due to repulsion between the dendritic branches. (C) Removing *Vang* functions in animals expressing *UAS-Wnt5* under the control of *Mz19-Gal4* return the VA1d dendrites to its compact morphology in the right AL. In the left AL, the two separated branches are closer together. (D, E) Adult ALs from animals expressing *Or88a-CD2* and *UAS-mCD8::GFP* under the control of *Mz19-Gal4* were stained with anti-CD2 (magenta) and anti-CD8 (green) to visualize the pre- and postsynaptic processes of the VA1d glomerulus. In the wild-type control, *Or88a* axons are faithfully paired with the VA1d dendrites (D). In animals expressing *UAS-Wnt5* under the control of *Mz19-Gal4* the *Or88a* axons were still correctly paired with the VA1d dendrites despite their splitting into two separated arbors (E). (F) Graph summarizing the percentage of intact VA1d glomeruli in wild-type and *Vang*⁶ animals overexpressing *Wnt5* in the VA1d glomeruli. (G) Graph summarizing the distance between the split VA1d arbors in wild-type and *Vang*⁶ animals overexpressing *Wnt5* in the VA1d glomeruli. Student's *t* test was used to compare the data of the wild-type and *Vang*⁶ animals overexpressing *Wnt5*. Scale bars: 10 μm.

<https://doi.org/10.1371/journal.pgen.1008767.g006>

Drl is differentially expressed by PN dendrites wherein it antagonizes *Wnt5*'s repulsion of the dendrites [11]. To delineate the AL region where *drl* functions, we examined the positioning of several glomeruli in the null *drl*² mutant by expressing *UAS-mCD8::GFP* under the control of various *Or-Gal4* drivers (Fig 8A–8I). We observed that, as in the *Vang* mutant, the lateral glomeruli showed the strongest displacements in positions compared with the control indicating that *drl* primarily regulates neurite targeting in the lateral AL (Fig 8A–8C). To better characterize the neuropil defect in this region we employed the *Crispr/Cas9* technique [30] to create the null *drl*^S allele on the *Mz19-Gal4* chromosome (Materials and Methods), which allowed us to assess the DA1/VA1d dendritic arrangement in the *drl* mutant. To our surprise, we observed that the DA1/VA1d dendritic pair in the *drl*^S/*drl*² null mutant showed strong deficits in DA1/VA1d rotation, resembling the *Wnt5*⁴⁰⁰ null phenotype (Fig 8J–8L). Indeed, measurement of the DA1/VA1d angle of the *drl*^S/*drl*² mutant ($76.55^\circ \pm 3.75^\circ$, N = 31) showed that it was even slightly larger than that of the *Wnt5*⁴⁰⁰ mutant ($69.22^\circ \pm 5.03^\circ$, N = 32, *t*-test $p = 0.2493$). The similarity of the *drl* and *Wnt5* mutant phenotypes indicates that *drl* cooperates with *Wnt5* in promoting the rotation of the DA1/VA1d glomeruli.

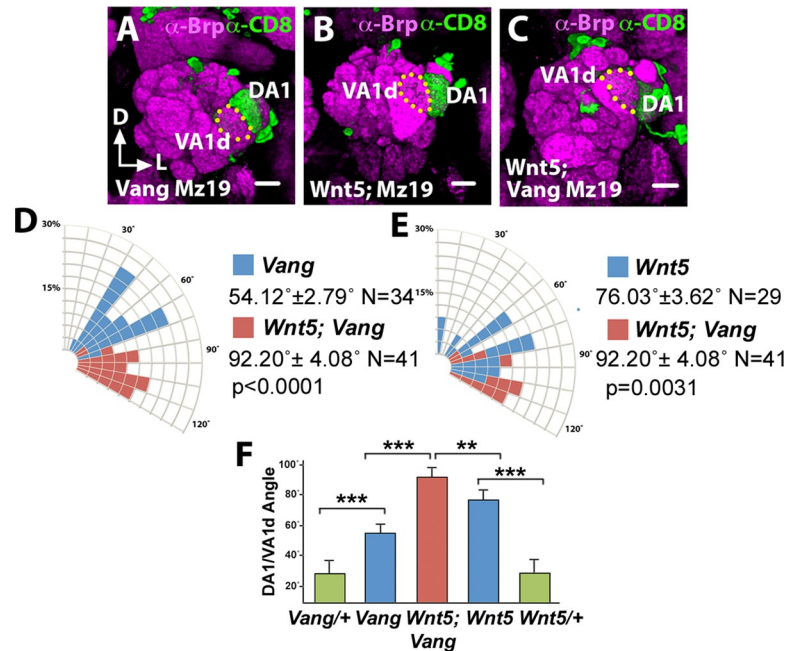


Fig 7. *Wnt5* and *Vang* could function independently to regulate DA1/VA1d glomerular rotation. (A–C) Frontal views of adult ALs from animals expressing *UAS-mCD8::GFP* under the control of *Mz19-Gal4* stained with antibodies against Brp (magenta) and CD8 (green) to visualize the glomerular pattern and the DA1/VA1d dendrites respectively, in the *Vang*⁶ (A), *Wnt5*⁴⁰⁰ (B) and *Wnt5*⁴⁰⁰; *Vang*⁶ (C) mutants. (D) Quantification of the DA1/VA1d angles in panels A and C showing that the rotational defect is stronger in the *Wnt5*⁴⁰⁰; *Vang*⁶ mutant than in the *Vang*⁶ mutant. (E) Quantification of the DA1/VA1d angles in B and C showing that the rotational defect is stronger in the *Wnt5*⁴⁰⁰; *Vang*⁶ mutant than in the *Wnt5*⁴⁰⁰ mutant. (F). Graph summarizing the DA1/VA1d angles in the *Vang*⁶ and *Wnt5*⁴⁰⁰ single mutants and *Wnt5*⁴⁰⁰; *Vang*⁶ double mutant. Student's *t* tests were used to compare the angles of the various mutants. Scale bars: 10 μ m.

<https://doi.org/10.1371/journal.pgen.1008767.g007>

drl acts in the DA1 dendrites to promote glomerular attraction to *Wnt5*

How does *drl* mediate *Wnt5* function in glomerular rotation? We hypothesized that *drl* functions in the DA1 dendrites, to regulate migration of the DA1 glomerulus towards the *Wnt5* source. In support of this idea, antibody staining of the Drl protein showed that it is highly expressed by the DA1 dendrites but not the VA1d dendrites (Fig 2D and 2E) [11]. The domain of high Drl expression occupies the anterior dorsolateral domain of the 24 hAPF ALs (0–8 μ m from anterior), a region in which *Wnt5* is also highly expressed [11]. The hypothesis predicts that ablation of *drl* in DA1 alone would disrupt the rotation of the DA1/VA1d glomeruli. To test this hypothesis, we used MARCM to induce *drl*^{1S} homozygosity in either DA1 or VA1d dendrites and assessed the effects on DA1/VA1d glomerular rotation. The DA1 and VA1 dendrites could be independently identified since their cell bodies are located in the lateral and anterodorsal PN clusters respectively. We observed that *drl*^{1S} mutant VA1d dendrites were associated with glomerular pairs with small angles (17.13° ± 3.68°, N = 16), that is, with the DA1 glomerulus closely associated with the dorsolateral AL (Fig 9C–9F). In contrast, *drl*^{1S} mutant DA1 dendrites are associated with glomeruli with wide variations in angles (58.43° ± 8.33°, N = 14, *t*-test *p* = 0.0003), that is, with the DA1 glomerulus not closely associated with the dorsolateral AL (Fig 9A, 9B, 9E and 9F). Thus, *drl* appears to act in the DA1 dendrites to confer directionality of the DA1 glomerulus towards the *Wnt5* source.

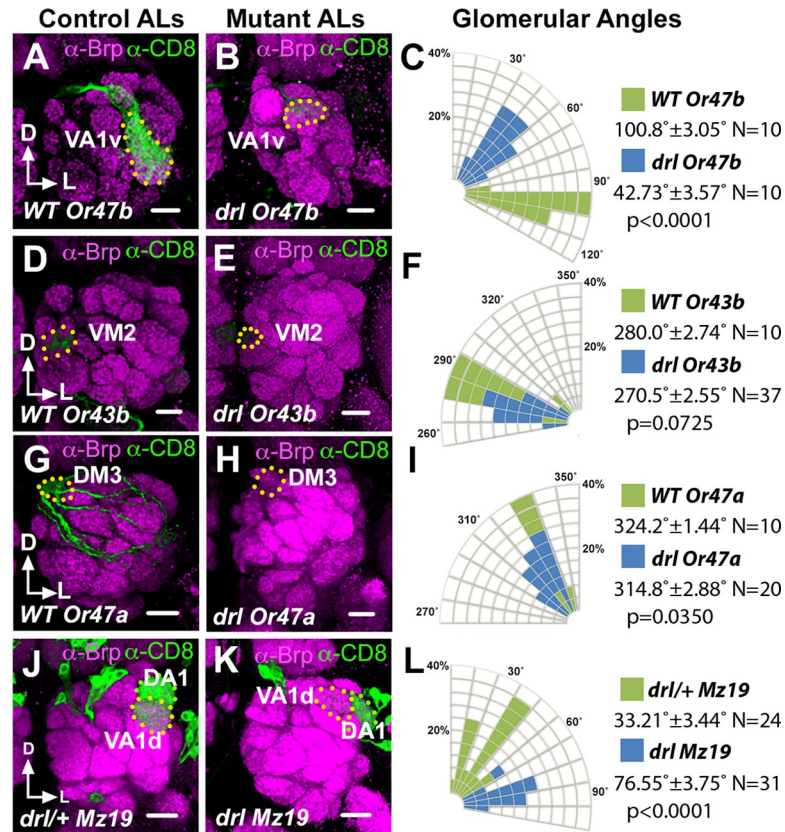


Fig 8. The *drl*² mutant AL defects resemble that of the *wnt5*⁴⁰⁰ mutant. (A–I) Left adult ALs from wild-type (A, B, G) and *drl*² (B, E, H) animals expressing *UAS-mCD8::GFP* under the control of *Or47b-Gal4* (A, B), *Or43b-Gal4* (D, E) and *Or47a-Gal4* (G, H) were stained with antibodies against Brp (Magenta) to highlight the AL neuropil and CD8 (green) to label lateral, medial and dorsal glomeruli respectively. (C, F, I) Quantification of the positions of the *Or47b*, *Or43b* and *Or47a* glomeruli respectively in the wild-type vs *drl*² animals. The glomeruli appeared to be displaced in the counterclockwise direction in the *drl*² mutant with VA1v showing the greatest displacement. (J, K) ALs from adult *drl*^{1S/+} control (J) and *drl*^{1S/drl}² animals (K) expressing *UAS-mCD8::GFP* under the control of *Mz19-Gal4* were stained with antibodies against Brp (Magenta) and CD8 (green) to highlight the AL neuropil and the DA1/VA1d PN dendritic arbors respectively. (L) Quantification of the DA1/VA1d angles in the *drl*^{1S/drl}² mutant. The DA1 dendrites are located lateral to the VA1d dendrites in the *drl*^{1S/drl}² mutant reflecting a severe impairment in DA1/VA1d dendritic rotation. This phenotype resembles that of the *Wnt5*⁴⁰⁰ mutant. Student's *t* tests were used to compare the data of the *drl* mutants with those of the controls. Scale bars: 10 μm.

<https://doi.org/10.1371/journal.pgen.1008767.g008>

drl likely converts *Wnt5* repulsion of the DA1 glomerulus into attraction

How does *drl* promote the migration of the DA1 glomerulus towards *Wnt5*? We propose two models by which *drl* could accomplish this task. In the first model, *drl* acts as a positive effector of *Wnt5* attractive signaling. In the second model, *drl* neutralizes *Wnt5* repulsive signaling and/or converts the repulsive signaling into an attractive one. Careful examination of the DA1/VA1d targeting defects in *drl*^{1S/drl}² null mutant revealed differences with that of the *Wnt5*⁴⁰⁰ mutant, inconsistent with the idea that *drl* acts as a positive effector of *Wnt5* signaling. First, the DA1 glomerulus is often displaced medially from the AL lateral border ($6.26 \mu\text{m} \pm 1.85 \mu\text{m}$ from border, $N = 28$) (Fig 10H), a defect not seen in the *Wnt5*⁴⁰⁰ mutant. This resulted in the frequent reversal in the positions of the DA1 and VA1d glomeruli (Fig 10B), or displacement of both glomeruli medially from the AL lateral border (Fig 10A). Second, the mean DA1/VA1d angle in the *drl*^{1S/drl}² null mutant is slightly but not significantly larger than that of *Wnt5*⁴⁰⁰ null mutant (Fig 10E and 10G). Instead the defects are

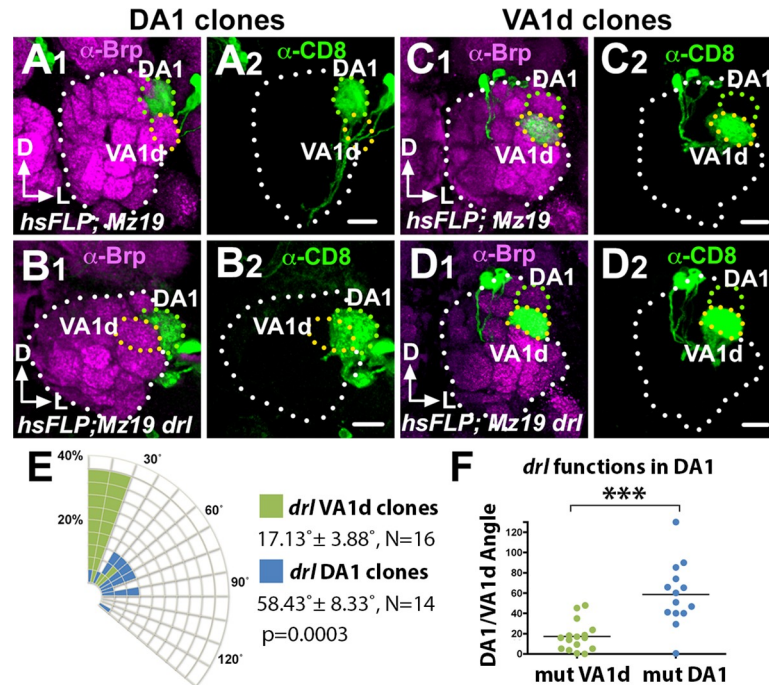


Fig 9. *drl* functions in the DA1 dendrites but not VA1d dendrites to promote DA1/VA1d glomerular rotation. Mosaic control and *drl*^{ΔS} ALs generated by the MARCM technique were stained with antibodies against Brp (Magenta) to visualize the glomerular pattern and CD8 (green) to visualize the clonal PN dendrites. (A) Control DA1 dendrites are often observed in DA1/VA1d glomerular pair with small rotational angles. (B) In contrast, *drl*^{ΔS} mutant DA1 dendrites are frequently observed in DA1/VA1d glomeruli with large rotational angles indicating impaired glomerular rotation. (C) Control VA1d dendrites are often observed in DA1/VA1d glomerular pair with small rotational angles. (D) Likewise, *drl*^{ΔS} mutant VA1d dendrites are frequently observed in DA1/VA1d glomerular pair with small rotational angles indicating normal glomerular rotation. (E) Quantification of the glomerular angles of the *drl*^{ΔS} mutant DA1 and VA1d clones. (F) Graph summarizing the *drl*^{ΔS} DA1 vs VA1d clonal data. Student's *t* test was used to compare the data of the *drl* DA1 vs VA1d mutant clones. Scale bars: 10 μ m.

<https://doi.org/10.1371/journal.pgen.1008767.g009>

more consistent with the second model, which predicts increased *Wnt5* repulsion of the DA1 glomerulus in the *drl* mutant, thus driving the glomerulus ventromedially. To test this hypothesis, we simultaneously removed both *drl* and *Wnt5* functions and examined the displacement of the DA1/VA1d glomeruli. We observed that the DA1 glomerulus is restored to AL lateral border in the *Wnt5*⁴⁰⁰; *drl*^{ΔS}/*drl*^{Δ2} double mutant, as it is in the *Wnt5* homozygote (0.00 μ m from border, N = 30 and N = 25 respectively) (Fig 10C and 10H). We also observed that the DA1/VA1d angle in the *Wnt5*; *drl* double mutant (70.66° ± 4.39°, N = 29) is more similar to that of the *Wnt5* mutant (69.22° ± 5.03°, N = 32, *t*-test p = 0.83) than that of the *drl* mutant (76.55° ± 3.75°, N = 31, *t*-test p = 0.3102) (Fig 10E and 10G). We conclude that *Wnt5* repels the DA1 glomerulus ventromedially and that *drl* antagonizes the *Wnt5* repulsive activity. Since we showed above that *drl* promotes the migration of DA1 towards *Wnt5*, we conclude that *drl* acts in the DA1 glomerulus to convert *Wnt5* repulsion of the DA1 glomerulus into attraction. Taken together, our results suggest that *Wnt5* orients the rotation of the VA1d/DA1 glomeruli by attracting the DA1 glomerulus through *Wnt5*-*drl* signaling and repelling the VA1d glomerulus through *Wnt5*-*Vang* signaling.

To investigate the mechanism by which *drl* converts *Wnt5* repulsion of the DA1 glomerulus into attraction, we examined the mechanism by which *Wnt5* repels the DA1 glomerulus. A likely scenario is that *Wnt5* repels the DA1 glomerulus through *Vang*. To test this idea, we simultaneously removed both *drl* and *Vang* functions and measured the displacement of the

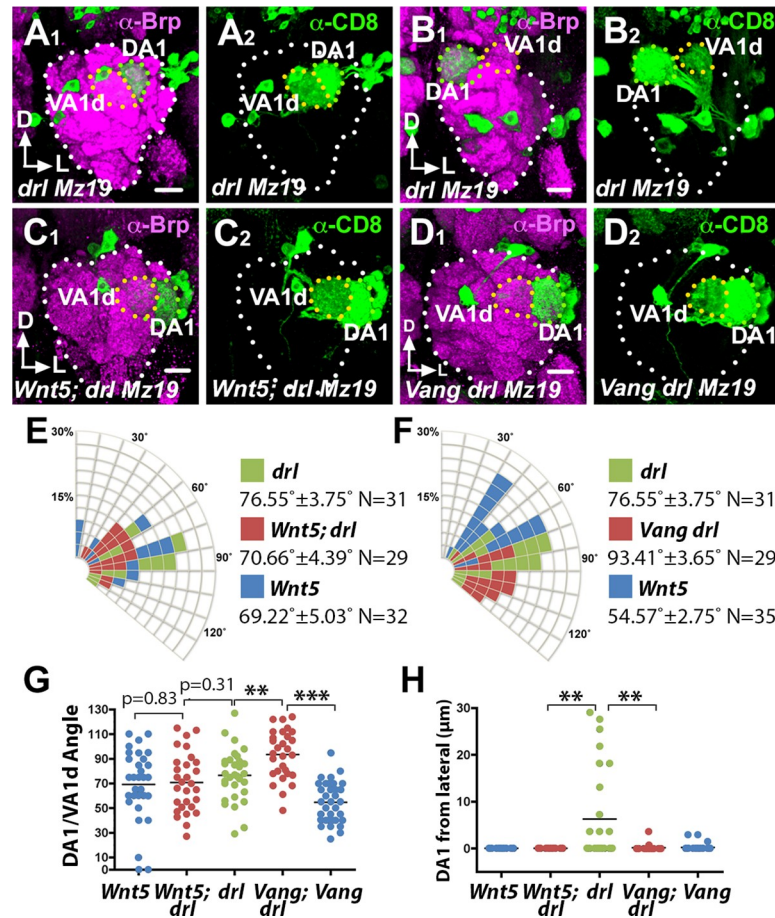


Fig 10. *Wnt5* repels the DA1 glomerulus through *Vang*, a function that *drl* antagonizes. Left adult ALs of animals expressing *UAS-mCD8::GFP* under the control of *Mz19-Gal4* were stained with nc82 (magenta) and anti-CD8 (green) to visualize the neuropil and the DA1/VA1d dendrites respectively. (A, B) In the *drl* mutant, the DA1 glomerulus was often displaced from the AL lateral border, resulting in the medial shift of the DA1/VA1d glomerular pair (A) or a reversal in the positions of the two glomeruli (B). (C) The loss of the *wnt5* gene suppressed the DA1 medial displacement, restoring the DA1 glomerulus to the AL lateral border, indicating that *drl* antagonizes *Wnt5* repulsion of the DA1 glomerulus. (D) The DA1 medial displacement is also suppressed by the loss of the *Vang* gene, suggesting that *Vang* functions in *Wnt5* repulsion of the DA1 glomerulus. In addition, the DA1/VA1d glomerular angle of the *drl* mutant is large. (E) Quantification of the DA1/VA1d glomerular angles in the *drl* and *Wnt5* single mutants and *Wnt5; drl* double mutant. (F) Quantification of the DA1/VA1d glomerular angles in the *drl* and *Vang drl* double mutant and *Vang* single mutant. (G) Graph summarizing the DA1/VA1d glomerular angles in the *drl*, *Wnt5*, and *Vang* mutants. (H) Graph summarizing the distance of the DA1 glomerulus from the AL lateral border in the *drl*, *Wnt5*, and *Vang* mutants. Student's *t* tests were used to compare the data of the double mutants with the single mutants. Scale bars: 10 μm.

<https://doi.org/10.1371/journal.pgen.1008767.g010>

DA1 glomerulus from the AL lateral border as well as the DA1/VA1d rotational angle. We found that in the *Vang⁶ drl^{1S}/Vang⁶ drl²* double mutant, the DA1 glomerulus is restored to the AL lateral border ($0.156 \mu\text{m} \pm 0.132 \mu\text{m}$, $N = 28$, *t*-test $p = 0.0017$) (Fig 10D and 10H). We conclude that *drl* neutralizes the *Wnt5*-*Vang* repulsion of the DA1 glomerulus. Interestingly, measurement of the DA1/VA1d angles in the *Vang drl* double mutant showed that the rotation of the glomeruli is more severely impaired ($93.41^\circ \pm 3.65^\circ$, $N = 29$) than that of either single mutants ($76.55^\circ \pm 3.75^\circ$ in *drl²*, $N = 31$, *t*-test $p = 0.0021$ and $54.57^\circ \pm 2.75^\circ$ in *Vang⁶*, $N = 35$, *t*-test $p < 0.0001$) (Fig 10F and 10G). The enhanced phenotype of the *Vang drl* double mutant indicated that *drl* and *Vang* act in parallel pathways to promote DA1/VA1d rotation. The

parallel functions are in accord with our model that *drl* acts in the DA1 glomerulus while *Vang* acts in the adjacent VA1d glomerulus to promote DA1/VA1d rotation. Simultaneous loss of *Vang* and *drl* would be expected to exacerbate the DA1/VA1d rotational defect.

Discussion

Elucidating the mechanisms that shape dendritic arbors is key to understanding the principles of nervous system assembly. Genetic approaches have revealed both intrinsic and extrinsic cues that regulate the patterning of dendritic arbors [31, 32]. In contrast, there are only a few reports on the roles of axons in shaping dendritic arborization [33, 34]. In this paper we provide evidence that final patterning of the fly olfactory map is the result of an interplay between ORN axons, PN dendrites and the Wnt5 directional signal (Fig 11). We show that the Vang PCP protein [20, 21] is an axon-derived factor that mediates the Wnt5 repulsion of the VA1d dendrites. We also show that the Drl protein is specifically expressed by the DA1 dendrites where it antagonizes the Wnt5-Vang repulsion of the DA1 glomerulus and likely converts it into an attractive response. The differential responses of the DA1 and VA1d glomeruli to Wnt5 would produce the forces by which Wnt5 effects the rotation of the glomerular pair. We present the following lines of evidence in support of this model of olfactory neural circuit development.

Immunostaining showed that Vang is expressed at the same time and place as Wnt5 and Drl, and concentrated in the dorsolateral AL where major dendritic reorganization occurs [11]. Mutations in *Vang* strongly disrupted the pattern of glomeruli in the AL, mimicking the *Wnt5* mutant phenotype. Notably, mutation of *Vang* suppressed the strong repulsion of the VA1d dendritic arbor caused by *Wnt5* overexpression, indicating that *Vang* acts downstream of *Wnt5* to repel the VA1d dendrites. Unexpectedly, using cell type-specific transgenic experiments and mosaic analyses we found that *Vang* functions specifically in the ORNs, indicating an obligatory codependence of ORN axon and PN dendritic targeting. Unlike the VA1d glomerulus, which expresses low levels of *drl* and is repelled by *Wnt5*, the adjacent DA1

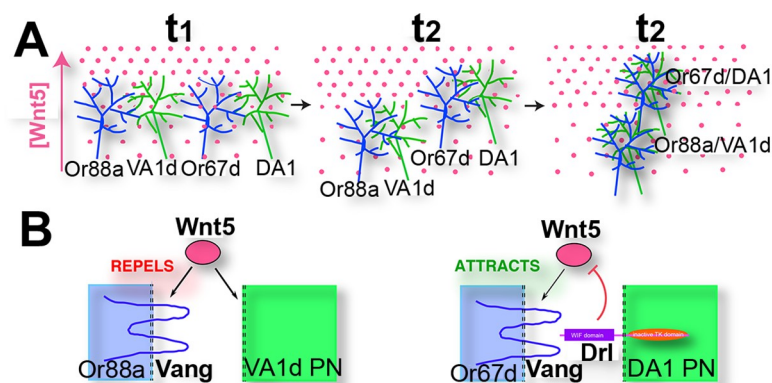


Fig 11. Model for the Wnt5-directed rotation of developing glomeruli. (A) The targeting of two ORN axons (Or88a and Or67d) on their respective PN dendritic partners (VA1d and DA1) in the Wnt5 gradient at three time points is depicted. At time t_1 , the pre- and postsynaptic processes have not paired up and the individual neurites do not respond to the Wnt5 signal. At time t_2 , the neurites are beginning to pair up, which allows the nascent synapses to respond to the Wnt5 signal. (B) The Or88a:VA1d glomerulus is repelled by Wnt5 because the VA1d dendrite does not express Drl. On the other hand, the Or67d:DA1 glomerulus is attracted by Wnt5 because the DA1 dendrite expresses Drl, which converts Wnt5-Vang repulsion into attraction. Repulsion of the Or88a:VA1d glomerulus causes it to move down the Wnt5 gradient while the attraction of the Or67d:DA1 glomerulus causes it to move up the Wnt5 gradient. At time t_3 , the ORN axons and PN dendrites have fully condensed to form glomeruli. The opposing responses of the glomeruli to Wnt5 result in their rotation around each other.

<https://doi.org/10.1371/journal.pgen.1008767.g011>

glomerulus expresses high levels of *drl*. Mosaic analyses showed that *drl* acts specifically in the DA1 dendrites to confer directionality of the DA1 glomerulus towards *Wnt5*. Finally, in the absence of *drl*, the DA1 glomerulus is displaced away from the *Wnt5* source, a defect that is suppressed by the removal of either *Wnt5* or *Vang*. Taken together, we propose that *drl* likely converts *Wnt5* repulsion of the DA1 glomerulus into attraction by inhibiting *Wnt5-Vang* repulsive signaling.

We envision that *Vang* and *Drl* act cell autonomously to regulate axonal and dendritic guidance respectively and cell non-autonomously to modulate each other's functions. Both *Vang* and *Drl/Ryk* have well-documented cell autonomous functions in neurite guidance. For example, vertebrate *Vangl2* was localized to the filopodia of growth cones [35, 36] and *Drosophila* *Vang* mediates the repulsion of mushroom body axon branches in response to *Wnt5* [29, 37]. Similarly, *Drl* and *Ryk* mediate the functions of *Wnt5* and *Wnt5a* respectively in the targeting of dendrites [16, 38] and axons [5, 14, 17, 39, 40]. Both proteins also have well-documented cell non-autonomous functions. Vertebrate *Vangl2* acts as a ligand to steer migrating neurons [41, 42]. We and others have shown that *Drl* could sequester *Wnt5* using its extracellular Wnt Inhibitory Factor (WIF) motif [38, 43–45]. Indeed, in this manner *Drl* may reduce *Wnt5-Vang* interaction, thus neutralizing *Wnt5* repulsion of the glomeruli. How would *Drl* convert a glomerulus's response to *Wnt5* from repulsion to attraction? Increasing *Ryk* levels were proposed to titrate out *Fz5* in chick retinal ganglion axons, thus converting growth cone response to *Wnt3* from attraction to repulsion [46]. Whether *Drl* function through a similar mechanism in the DA1 dendrites will require further investigation.

The opposing functions of *Vang* and *Drl* in a migrating glomerulus satisfies Geirer's postulate for topographic mapping, which states that targeting neurites must detect two opposing forces in the target so that each neurite would come to rest at the point where the opposing forces cancel out [47]. Thus, the relative levels of *Drl* and *Vang* activities in a glomerulus may determine its targeting position in the *Wnt5* gradient (Fig 11). For the DA1/VA1d glomerular pair, the relative levels of *Drl* and *Vang* activities would result in the migration of DA1 up the gradient and VA1d down the gradient, that is, the rotation of the glomerular pair. The opposing effects of *Wnt5* on the targeting glomeruli could allow the single *Wnt5* gradient to refine the pattern of the olfactory map.

The rotation of the DA1/VA1d glomeruli bears intriguing resemblance to the PCP-directed rotation of multicellular structures such as mouse hair follicles and fly ommatidia, whose mechanisms remain incompletely understood [48–50]. Our demonstration of the push-pull effect of *Wnt5* on the glomeruli suggests that similar mechanisms may be involved in other PCP-directed rotations. Planar polarity signaling has emerged as an important mechanism in the morphogenesis of many tissues [20, 51, 52]. However, apart from the molecules of the core PCP group (*Vang*, *Prickle*, *Frizzled* and *Dishevelled*) the identities of other signaling components are subjects of debate. A key question is the extracellular cue that aligns the core PCP proteins with the global tissue axes. Although *Wnt* ligands have been implicated, a definitive link between them and PCP signaling has been difficult to establish [20, 21, 53]. Our work showing that *Wnt5* and *Vang* act together to direct the orientation of nascent glomeruli adds to two other reports [54, 55] that *Wnt* proteins play instructive roles in PCP signaling. Another debate surrounds the role of *Drl/Ryk* role in PCP signaling. First identified as signal transducing receptors for a subset of *Wnt* ligands in *Drosophila* [17, 56], vertebrate *Ryk* was subsequently shown to act in PCP signaling [57, 58]. These reports, combined with the lack of classical wing-hair PCP phenotypes in the *drl* mutant, led to the proposal that *Ryk*'s PCP function is a vertebrate innovation [59]. Our demonstration of *drl*'s role in *Wnt5-Vang* signaling suggests, however, that the *Drl/Ryk*'s PCP function is likely to be evolutionarily ancient.

Materials and methods

Fly strains and Crispr/Cas9 knockout of the *drl* gene

All mutant and transgenic fly lines were obtained from the Bloomington *Drosophila* Stock Center except for *UAS-Vang*, which was a gift from B. A. Hassan. The *Wnt5⁴⁰⁰* allele is a null allele generated by the imprecise excision of an adjacent P element, resulting in the deletion of most of the *Wnt5* open reading frame [14]. The *drl²* allele is a null allele generated by the imprecise excision of a P element in the 5' non-coding region, resulting in the deletion of the 5' regulatory sequences and the first exon of *drl* [60]. To generate a new *drl* null allele on the *Mz19-Gal4* chromosome, exons 2, 3 and 4 of the *drl* locus (encompassing ~90% of the *drl* open reading frame) were excised from the chromosome by Crispr/Cas9-mediated deletion using the sgRNAs GACAAGTGAAGGGGTGCTGT and GACACCTGTAGTGAGAGGTA following a published protocol [61]. Ten individual offspring from Crispr/Cas9 fathers were crossed to *Adv/CyO* virgins to establish lines. The lines were screened by PCR using deletion-spanning primers to identify potential *drl* mutants. The PCR products were sequenced and one mutant, *drl^{1S}*, with the expected precise deletion of the *drl* locus in the *Mz19-Gal4* background was chosen for study. The *drl^{1S}* mutation failed to complement the AL phenotype of the *drl²* mutation, consistent with *drl^{1S}* being a null allele.

Clonal analyses

To induce *Vang* mutant ORNs, adults of the following genotype, *ey-FLP/+; FRT42 w⁺ cl/Mz19-Gal4 FRT42 Vang⁶ or (+)*, were obtained and dissected. To induce *Vang* and *drl* mutant PN, the MARCM technique was employed [28]. Third instar larvae of the following genotypes: *hs-FLP UAS-mCD8::GFP/+; FRT42 tub-Gal80/FRT42 GH146-Gal4 Vang⁶ or (+)* and *hs-FLP UAS-mCD8::GFP/+; FRT40 tub-Gal80/FRT40 Mz19-Gal4 drl^{1S} or (+); UAS-mCD8::GFP/+* were heat-shocked at 37°C for 40 minutes. Adult brains were dissected and processed as described below.

Immunohistochemistry

Dissection, fixing and staining of adult or pupal brains were performed as previously described [27, 62]. Rabbit anti-DRL (1:1000) was a generous gift from J. M. Dura; rat anti-Vang (1:500) was a gift from D. Strutt; mAb nc82 (1:20) [63] was obtained from the Iowa Antibody Bank; rat anti-mCD8 mAb (1:100) was obtained from Caltag. The secondary antibodies, FITC-conjugated goat anti-rabbit, Cy3-conjugated goat anti-mouse and FITC-conjugated goat anti-rat, were obtained from Jackson Laboratories and used at 1:100 dilutions. The stained brains were imaged using a Zeiss 710 confocal microscope.

Quantification of glomerular rotation

Two different quantification strategies were employed. To quantify the displacements of single glomeruli labeled by the *Or-Gal4* drivers [6], the angle subtended at the VA6 glomerulus (close to the center of the AL) by the dorsal pole and the labeled glomerulus (in the dorsal/0° → lateral/90° → ventral/180° → medial direction/270°) was measured. To quantify the rotation of the DA1 and VA1d glomeruli [22] around each other, the angle subtended at the VA1d glomerulus by the dorsal pole and the DA1 glomerulus (in the dorsal/0° → lateral/90° → ventral/180° → medial/270° direction) was measured. Data were collected, analyzed and plotted using the Prism statistical software. For two-sample comparisons, unpaired Student's *t*-tests were applied. For comparisons among more than two groups, one-way ANOVA tests were used followed by Tukey's test. Rose diagrams were plotted using the Excel program.

Supporting information

S1 Fig. Method for quantifying the rotation of the DA1 and VA1d glomeruli around each other. Schematic representations of the frontal views of left ALs are shown (dorsal/0° is up and lateral/90° is to the right). A line was drawn through the centers of the DA1 and VA1d glomeruli. Where the line intersects with the dorsal-ventral axis, the angle in the clockwise direction from 0° was measured. During development, the DA1/VA1d angle decreases because the two glomeruli rotate around each other in the counterclockwise direction. (TIF)

S2 Fig. Overexpression of *Wnt5* in the DA1 and VA1d dendrites does not disrupt ORN differentiation or survival. Frontal views of adult left antennae are shown (dorsal up and lateral to the right). (A-C) Representative freshly dissected antennae from animals expressing *Or88a-mGFP* were imaged using the confocal microscope to visualize the live *Or88a* neurons in the wild-type (A), *Wnt5⁴⁰⁰* (B), and *Mz19-Gal4 UAS-Wnt5* (C) animals. (D) Quantification of the *Or88a* neuronal numbers in the different genotypes. The numbers of *Or88a* neurons in the *Wnt5⁴⁰⁰* (41.22 ± 2.681 , N = 9) mutant and *Mz19-Gal4 UAS-Wnt5* (32.00 ± 1.535 , N = 8) overexpression animals are similar to those in the Wild type (33.17 ± 0.8776 , N = 12). Wild type vs *Wnt5⁴⁰⁰*, $p = 0.0060$; Wild type vs *Mz19-Gal4 UAS-Wnt5*, $p = 0.8834$; *Wnt5⁴⁰⁰* vs *Mz19-Gal4 UAS-Wnt5*, $p = 0.0043$; one-way ANOVA with post hoc Tukey test. (TIF)

Acknowledgments

We thank L. Luo and the Bloomington Stock Center for providing fly stocks, J. M. Dura and D. Strutt for their generous gifts of the anti-Drl and anti-Vang antibodies respectively, and J. N. Noordermeer and J. M. Dura for their comments on the paper.

Author Contributions

Conceptualization: Huey Hing.

Data curation: Huey Hing.

Formal analysis: Huey Hing, Lee G. Fradkin.

Funding acquisition: Huey Hing.

Investigation: Huey Hing, Noah Reger, Jennifer Snyder, Lee G. Fradkin.

Methodology: Huey Hing.

Project administration: Huey Hing.

Resources: Huey Hing.

Software: Huey Hing.

Supervision: Huey Hing.

Validation: Huey Hing.

Visualization: Huey Hing.

Writing – original draft: Huey Hing.

Writing – review & editing: Huey Hing, Lee G. Fradkin.

References

1. Hong W, Luo L. Genetic control of wiring specificity in the fly olfactory system. *Genetics*. 2014; 196(1):17–29. <https://doi.org/10.1534/genetics.113.154336> PMID: 24395823
2. Luo L, Flanagan JG. Development of continuous and discrete neural maps. *Neuron*. 2007; 56(2):284–300. <https://doi.org/10.1016/j.neuron.2007.10.014> PMID: 17964246
3. McLaughlin T, O'Leary DD. Molecular gradients and development of retinotopic maps. *Annu Rev Neurosci*. 2005; 28:327–55. <https://doi.org/10.1146/annurev.neuro.28.061604.135714> PMID: 16022599
4. Sakano H. Neural map formation in the mouse olfactory system. *Neuron*. 2010; 67(4):530–42. <https://doi.org/10.1016/j.neuron.2010.07.003> PMID: 20797531
5. Sarin S, Zuniga-Sanchez E, Kurmangaliyev YZ, Cousins H, Patel M, Hernandez J, et al. Role for Wnt Signaling in Retinal Neuropil Development: Analysis via RNA-Seq and In Vivo Somatic CRISPR Mutagenesis. *Neuron*. 2018; 98(1):109–26 e8. <https://doi.org/10.1016/j.neuron.2018.03.004> PMID: 29576390
6. Couto A, Alenius M, Dickson BJ. Molecular, anatomical, and functional organization of the *Drosophila* olfactory system. *Curr Biol*. 2005; 15(17):1535–47. <https://doi.org/10.1016/j.cub.2005.07.034> PMID: 16139208
7. Fishilevich E, Vosshall LB. Genetic and functional subdivision of the *Drosophila* antennal lobe. *Curr Biol*. 2005; 15(17):1548–53. <https://doi.org/10.1016/j.cub.2005.07.066> PMID: 16139209
8. Jefferis GS, Vyas RM, Berdnik D, Ramaekers A, Stocker RF, Tanaka NK, et al. Developmental origin of wiring specificity in the olfactory system of *Drosophila*. *Development*. 2004; 131(1):117–30. <https://doi.org/10.1242/dev.00896> PMID: 14645123
9. Komiyama T, Sweeney LB, Schuldiner O, Garcia KC, Luo L. Graded expression of semaphorin-1a cell-autonomously directs dendritic targeting of olfactory projection neurons. *Cell*. 2007; 128(2):399–410. <https://doi.org/10.1016/j.cell.2006.12.028> PMID: 17254975
10. Sweeney LB, Chou YH, Wu Z, Joo W, Komiyama T, Potter CJ, et al. Secreted semaphorins from degenerating larval ORN axons direct adult projection neuron dendrite targeting. *Neuron*. 2011; 72(5):734–47. <https://doi.org/10.1016/j.neuron.2011.09.026> PMID: 22153371
11. Wu Y, Helt JC, Wexler E, Petrova IM, Noordermeer JN, Fradkin LG, et al. Wnt5 and drl/ryk gradients pattern the *Drosophila* olfactory dendritic map. *J Neurosci*. 2014; 34(45):14961–72. <https://doi.org/10.1523/JNEUROSCI.2676-14.2014> PMID: 25378162
12. Jhaveri D, Sen A, Rodrigues V. Mechanisms underlying olfactory neuronal connectivity in *Drosophila*—the atonal lineage organizes the periphery while sensory neurons and glia pattern the olfactory lobe. *Dev Biol*. 2000; 226(1):73–87. <https://doi.org/10.1006/dbio.2000.9855> PMID: 10993675
13. Rodrigues V, Hummel T. Development of the *Drosophila* olfactory system. *Adv Exp Med Biol*. 2008; 628:82–101. https://doi.org/10.1007/978-0-387-78261-4_6 PMID: 18683640
14. Fradkin LG, van Schie M, Wouda RR, de Jong A, Kamphorst JT, Radjkoemar-Bansraj M, et al. The *Drosophila* Wnt5 protein mediates selective axon fasciculation in the embryonic central nervous system. *Dev Biol*. 2004; 272(2):362–75. <https://doi.org/10.1016/j.ydbio.2004.04.034> PMID: 15282154
15. Harris KE, Beckendorf SK. Different Wnt signals act through the Frizzled and RYK receptors during *Drosophila* salivary gland migration. *Development*. 2007; 134(11):2017–25. <https://doi.org/10.1242/dev.001164> PMID: 17507403
16. Yasunaga K, Tezuka A, Ishikawa N, Dairyo Y, Togashi K, Koizumi H, et al. Adult *Drosophila* sensory neurons specify dendritic territories independently of dendritic contacts through the Wnt5-Drl signaling pathway. *Genes Dev*. 2015; 29(16):1763–75. <https://doi.org/10.1101/gad.262592.115> PMID: 26302791
17. Yoshikawa S, McKinnon RD, Kokel M, Thomas JB. Wnt-mediated axon guidance via the *Drosophila* Derailed receptor. *Nature*. 2003; 422(6932):583–8. <https://doi.org/10.1038/nature01522> PMID: 12660735
18. Taylor J, Abramova N, Charlton J, Adler PN. Van Gogh: a new *Drosophila* tissue polarity gene. *Genetics*. 1998; 150(1):199–210. PMID: 9725839
19. Wolff T, Rubin GM. Strabismus, a novel gene that regulates tissue polarity and cell fate decisions in *Drosophila*. *Development*. 1998; 125(6):1149–59. PMID: 9463361
20. Goodrich LV, Strutt D. Principles of planar polarity in animal development. *Development*. 2011; 138(10):1877–92. <https://doi.org/10.1242/dev.054080> PMID: 21521735
21. Yang Y, Mlodzik M. Wnt-Frizzled/planar cell polarity signaling: cellular orientation by facing the wind (Wnt). *Annu Rev Cell Dev Biol*. 2015; 31:623–46. <https://doi.org/10.1146/annurev-cellbio-100814-125315> PMID: 26566118

22. Ito K, Suzuki K, Estes P, Ramaswami M, Yamamoto D, Strausfeld NJ. The organization of extrinsic neurons and their implications in the functional roles of the mushroom bodies in *Drosophila melanogaster* Meigen. *Learn Mem.* 1998; 5(1–2):52–77. PMID: [10454372](#)
23. Zhu H, Luo L. Diverse functions of N-cadherin in dendritic and axonal terminal arborization of olfactory projection neurons. *Neuron.* 2004; 42(1):63–75. [https://doi.org/10.1016/s0896-6273\(04\)00142-4](https://doi.org/10.1016/s0896-6273(04)00142-4) PMID: [15066265](#)
24. Strutt H, Strutt D. Differential stability of flamingo protein complexes underlies the establishment of planar polarity. *Curr Biol.* 2008; 18(20):1555–64. <https://doi.org/10.1016/j.cub.2008.08.063> PMID: [18804371](#)
25. Robinow S, White K. Characterization and spatial distribution of the ELAV protein during *Drosophila melanogaster* development. *J Neurobiol.* 1991; 22(5):443–61. <https://doi.org/10.1002/neu.480220503> PMID: [1716300](#)
26. Ni JQ, Zhou R, Czech B, Liu LP, Holderbaum L, Yang-Zhou D, et al. A genome-scale shRNA resource for transgenic RNAi in *Drosophila*. *Nat Methods.* 2011; 8(5):405–7. <https://doi.org/10.1038/nmeth.1592> PMID: [21460824](#)
27. Ang LH, Kim J, Stepensky V, Hing H. Dock and Pak regulate olfactory axon pathfinding in *Drosophila*. *Development.* 2003; 130(7):1307–16. <https://doi.org/10.1242/dev.00356> PMID: [12588847](#)
28. Lee T, Luo L. Mosaic analysis with a repressible cell marker for studies of gene function in neuronal morphogenesis. *Neuron.* 1999; 22(3):451–61. [https://doi.org/10.1016/s0896-6273\(00\)80701-1](https://doi.org/10.1016/s0896-6273(00)80701-1) PMID: [10197526](#)
29. Shimizu K, Sato M, Tabata T. The Wnt5/planar cell polarity pathway regulates axonal development of the *Drosophila* mushroom body neuron. *J Neurosci.* 2011; 31(13):4944–54. <https://doi.org/10.1523/JNEUROSCI.0154-11.2011> PMID: [21451033](#)
30. Gratz SJ, Cummings AM, Nguyen JN, Hamm DC, Donohue LK, Harrison MM, et al. Genome engineering of *Drosophila* with the CRISPR RNA-guided Cas9 nuclease. *Genetics.* 2013; 194(4):1029–35. <https://doi.org/10.1534/genetics.113.152710> PMID: [23709638](#)
31. Dong X, Shen K, Bulow HE. Intrinsic and extrinsic mechanisms of dendritic morphogenesis. *Annu Rev Physiol.* 2015; 77:271–300. <https://doi.org/10.1146/annurev-physiol-021014-071746> PMID: [25386991](#)
32. Valnegri P, Puram SV, Bonni A. Regulation of dendrite morphogenesis by extrinsic cues. *Trends Neurosci.* 2015; 38(7):439–47. <https://doi.org/10.1016/j.tins.2015.05.003> PMID: [26100142](#)
33. Altman J, Anderson WJ. Experimental reorganization of the cerebellar cortex. I. Morphological effects of elimination of all microneurons with prolonged x-irradiation started at birth. *J Comp Neurol.* 1972; 146(3):355–406. <https://doi.org/10.1002/cne.901460305> PMID: [5086676](#)
34. Ramirez-Suarez NJ, Belalcázar HM, Salazar CJ, Beyaz B, Raja B, Nguyen KCQ, et al. Axon-Dependent Patterning and Maintenance of Somatosensory Dendritic Arbors. *Dev Cell.* 2019; 48(2):229–44 e4. <https://doi.org/10.1016/j.devcel.2018.12.015> PMID: [30661986](#)
35. Onishi K, Shafer B, Lo C, Tissir F, Goffinet AM, Zou Y. Antagonistic functions of Dishevelleds regulate Frizzled3 endocytosis via filopodia tips in Wnt-mediated growth cone guidance. *J Neurosci.* 2013; 33(49):19071–85. <https://doi.org/10.1523/JNEUROSCI.2800-13.2013> PMID: [24305805](#)
36. Shafer B, Onishi K, Lo C, Colakoglu G, Zou Y. Vangl2 promotes Wnt/planar cell polarity-like signaling by antagonizing Dvl1-mediated feedback inhibition in growth cone guidance. *Dev Cell.* 2011; 20(2):177–91. <https://doi.org/10.1016/j.devcel.2011.01.002> PMID: [21316586](#)
37. Gombos R, Migh E, Antal O, Mukherjee A, Jenny A, Mihaly J. The Formin DAAM Functions as Molecular Effector of the Planar Cell Polarity Pathway during Axonal Development in *Drosophila*. *J Neurosci.* 2015; 35(28):10154–67. <https://doi.org/10.1523/JNEUROSCI.3708-14.2015> PMID: [26180192](#)
38. Sakurai M, Aoki T, Yoshikawa S, Santschi LA, Saito H, Endo K, et al. Differentially expressed Drl and Drl-2 play opposing roles in Wnt5 signaling during *Drosophila* olfactory system development. *J Neurosci.* 2009; 29(15):4972–80. <https://doi.org/10.1523/JNEUROSCI.2821-08.2009> PMID: [19369566](#)
39. Li L, Hutchins BI, Kalil K. Wnt5a induces simultaneous cortical axon outgrowth and repulsive axon guidance through distinct signaling mechanisms. *J Neurosci.* 2009; 29(18):5873–83. <https://doi.org/10.1523/JNEUROSCI.0183-09.2009> PMID: [19420254](#)
40. Liu Y, Shi J, Lu CC, Wang ZB, Lyuksytova AI, Song XJ, et al. Ryk-mediated Wnt repulsion regulates posterior-directed growth of corticospinal tract. *Nat Neurosci.* 2005; 8(9):1151–9. <https://doi.org/10.1038/nn1520> PMID: [16116452](#)
41. Davey CF, Mathewson AW, Moens CB. PCP Signaling between Migrating Neurons and their Planar-Polarized Neuroepithelial Environment Controls Filopodial Dynamics and Directional Migration. *PLoS Genet.* 2016; 12(3):e1005934. <https://doi.org/10.1371/journal.pgen.1005934> PMID: [26990447](#)
42. Ghimire SR, Ratzan EM, Deans MR. A non-autonomous function of the core PCP protein VANGL2 directs peripheral axon turning in the developing cochlea. *Development.* 2018; 145(12).

43. Grillenzoni N, Flandre A, Lasbleiz C, Dura JM. Respective roles of the DRL receptor and its ligand WNT5 in *Drosophila* mushroom body development. *Development*. 2007; 134(17):3089–97. <https://doi.org/10.1242/dev.02876> PMID: 17652353
44. Reynaud E, Lahaye LL, Boulanger A, Petrova IM, Marquilly C, Flandre A, et al. Guidance of *Drosophila* Mushroom Body Axons Depends upon DRL-Wnt Receptor Cleavage in the Brain Dorsomedial Lineage Precursors. *Cell Rep*. 2015; 11(8):1293–304. <https://doi.org/10.1016/j.celrep.2015.04.035> PMID: 25981040
45. Yao Y, Wu Y, Yin C, Ozawa R, Aigaki T, Wouda RR, et al. Antagonistic roles of Wnt5 and the Drl receptor in patterning the *Drosophila* antennal lobe. *Nat Neurosci*. 2007; 10(11):1423–32. <https://doi.org/10.1038/nn1993> PMID: 17934456
46. Schmitt AM, Shi J, Wolf AM, Lu CC, King LA, Zou Y. Wnt-Ryk signalling mediates medial-lateral retinotectal topographic mapping. *Nature*. 2006; 439(7072):31–7. <https://doi.org/10.1038/nature04334> PMID: 16280981
47. Gierer. Directional cues for growing axons forming the retinotectal projection. *Development*. 1987; 101:479–89.
48. Devenport D, Fuchs E. Planar polarization in embryonic epidermis orchestrates global asymmetric morphogenesis of hair follicles. *Nat Cell Biol*. 2008; 10(11):1257–68. <https://doi.org/10.1038/ncb1784> PMID: 18849982
49. Mlodzik M. Planar polarity in the *Drosophila* eye: a multifaceted view of signaling specificity and cross-talk. *EMBO J*. 1999; 18(24):6873–9. <https://doi.org/10.1093/emboj/18.24.6873> PMID: 10601009
50. Reifegerste R, Moses K. Genetics of epithelial polarity and pattern in the *Drosophila* retina. *Bioessays*. 1999; 21(4):275–85. [https://doi.org/10.1002/\(SICI\)1521-1878\(199904\)21:4<275::AID-BIES3>3.0.CO;2-5](https://doi.org/10.1002/(SICI)1521-1878(199904)21:4<275::AID-BIES3>3.0.CO;2-5) PMID: 10377890
51. Daulat AM, Borg JP. Wnt/Planar Cell Polarity Signaling: New Opportunities for Cancer Treatment. *Trends Cancer*. 2017; 3(2):113–25. <https://doi.org/10.1016/j.trecan.2017.01.001> PMID: 28718442
52. Humphries AC, Mlodzik M. From instruction to output: Wnt/PCP signaling in development and cancer. *Curr Opin Cell Biol*. 2018; 51:110–6. <https://doi.org/10.1016/j.ceb.2017.12.005> PMID: 29289896
53. Wu J, Mlodzik M. Wnt/PCP Instructions for Cilia in Left-Right Asymmetry. *Dev Cell*. 2017; 40(5):423–4. <https://doi.org/10.1016/j.devcel.2017.02.023> PMID: 28292419
54. Minegishi K, Hashimoto M, Ajima R, Takaoka K, Shinohara K, Ikawa Y, et al. A Wnt5 Activity Asymmetry and Intercellular Signaling via PCP Proteins Polarize Node Cells for Left-Right Symmetry Breaking. *Dev Cell*. 2017; 40(5):439–52 e4. <https://doi.org/10.1016/j.devcel.2017.02.010> PMID: 28292423
55. Wu J, Roman AC, Carvajal-Gonzalez JM, Mlodzik M. Wg and Wnt4 provide long-range directional input to planar cell polarity orientation in *Drosophila*. *Nat Cell Biol*. 2013; 15(9):1045–55. <https://doi.org/10.1038/ncb2806> PMID: 23912125
56. Fradkin LG, Dura JM, Noordermeer JN. Ryks: new partners for Wnts in the developing and regenerating nervous system. *Trends Neurosci*. 2010; 33(2):84–92. <https://doi.org/10.1016/j.tins.2009.11.005> PMID: 20004982
57. Andre P, Wang Q, Wang N, Gao B, Schilit A, Halford MM, et al. The Wnt coreceptor Ryk regulates Wnt/planar cell polarity by modulating the degradation of the core planar cell polarity component Vangl2. *J Biol Chem*. 2012; 287(53):44518–25. <https://doi.org/10.1074/jbc.M112.414441> PMID: 23144463
58. Macheda ML, Sun WW, Kugathasan K, Hogan BM, Bower NI, Halford MM, et al. The Wnt receptor Ryk plays a role in mammalian planar cell polarity signaling. *J Biol Chem*. 2012; 287(35):29312–23. <https://doi.org/10.1074/jbc.M112.362681> PMID: 22773843
59. Yang W, Garrett L, Feng D, Elliott G, Liu X, Wang N, et al. Wnt-induced Vangl2 phosphorylation is dose-dependently required for planar cell polarity in mammalian development. *Cell Res*. 2017; 27(12):1466–84. <https://doi.org/10.1038/cr.2017.127> PMID: 29056748
60. Dura JM, Taillebourg E, Preat T. The *Drosophila* learning and memory gene *linotte* encodes a putative receptor tyrosine kinase homologous to the human RYK gene product. *FEBS Lett*. 1995; 370(3):250–4. [https://doi.org/10.1016/0014-5793\(95\)00847-3](https://doi.org/10.1016/0014-5793(95)00847-3) PMID: 7656987
61. Port F, Chen HM, Lee T, Bullock SL. Optimized CRISPR/Cas tools for efficient germline and somatic genome engineering in *Drosophila*. *Proc Natl Acad Sci U S A*. 2014; 111(29):E2967–76. <https://doi.org/10.1073/pnas.1405500111> PMID: 25002478
62. Ang LH, Chen W, Yao Y, Ozawa R, Tao E, Yonekura J, et al. Lim kinase regulates the development of olfactory and neuromuscular synapses. *Dev Biol*. 2006; 293(1):178–90. <https://doi.org/10.1016/j.ydbio.2006.01.030> PMID: 16529736
63. Wagh DA, Rasse TM, Asan E, Hofbauer A, Schwenkert I, Durrbeck H, et al. Bruchpilot, a protein with homology to ELKS/CAST, is required for structural integrity and function of synaptic active zones in *Drosophila*. *Neuron*. 2006; 49(6):833–44. <https://doi.org/10.1016/j.neuron.2006.02.008> PMID: 16543132